ficiency achieved in our first proof-of-principle experiment, which already compares well with state-of-the-art absorbing single-photon detectors (*20*–*22*).

The probability that an impinging photon is reflected is on average 66(2)%. If a photon is absorbed, the atomic state is projected, and the detection process gives the wrong result with a probability of 50%. Therefore, the probability to detect a single input photon without postselection on its reflection from the cavity is calculated to be 74% (*15*).

In contrast to all absorbing detectors, the efficiency of our detector can be further improved by attempting more measurements. Concatenating two of our devices is expected to increase the detection efficiency to 87%, whereas three or more devices should yield 89% (*15*). The achieved value is currently limited by absorption and scattering losses of both the atom and the cavity mirrors. To further improve, a decrease in cavity loss or an increase in atom-cavity coupling strength would be required. Both can be achieved either in Fabry-Perot (*23*) or other (*24*–*26*) resonators.

The atom-photon interaction mechanism that has been presented in this work lays the ground work for numerous experiments. A first step is the repeated nondestructive measurement of a single optical photon. Next, with a higher number of photons in the impinging laser pulse, the odd-even parity measurement allows one to generate new quantum states of optical light fields, such as Schrödinger-cat states (*27*). Measuring the phase of the reflected light could be used to entangle two atoms in the cavity (*28*). Moreover, using the polarization degree of freedom as a qubit should facilitate a deterministic quantum gate between a single photon and a single atom (*9*, *13*). This can be further extended to an entangling gate between several successively impinging photons (*9*) or between several atoms trapped in the same or even in remote cavities, thus efficiently generating atomic cluster states (*13*, *29*, *30*). Implementing this gate operation would also allow for a deterministic photonic Bell-state measurement, which would increase the efficiency of measurement-based quantum networks with remote single atoms (*31*, *32*) close to unity.

References and Notes

1. R. J. Glauber, *Phys. Rev.* **130**, 2529–2539 (1963).
2. L. Mandel, E. Wolf, *Optical Coherence and Quantum Optics* (Cambridge Univ. Press, Cambridge, 1995).
3. V. B. Braginsky, F. Y. Khalili, *Rev. Mod. Phys.* **68**, 1–11 (1996).
4. P. Grangier, J. A. Levenson, J.-P. Poizat, *Nature* **396**, 537–542 (1998).
5. H. M. Wiseman, G. J. Milburn, *Quantum Measurement and Control* (Cambridge Univ. Press, Cambridge, 2009).
6. J. L. O'Brien, *Science* **318**, 1567–1570 (2007).
7. N. Gisin, R. Thew, *Nat. Photonics* **1**, 165–171 (2007).
8. H. J. Kimble, *Nature* **453**, 1023–1030 (2008).
9. L.-M. Duan, H. J. Kimble, *Phys. Rev. Lett.* **92**, 127902 (2004).
10. G. Nogues *et al.*, *Nature* **400**, 239–242 (1999).
11. C. Guerlin *et al.*, *Nature* **448**, 889–893 (2007).
12. B. R. Johnson *et al.*, *Nat. Phys.* **6**, 663–667 (2010).
13. J. Cho, H.-W. Lee, *Phys. Rev. Lett.* **95**, 160501 (2005).
14. J. Bochmann *et al.*, *Phys. Rev. Lett.* **104**, 203601 (2010).
15. Materials and methods are available as supplementary materials on *Science* Online.
16. A. Reiserer, C. Nölleke, S. Ritter, G. Rempe, *Phys. Rev. Lett.* **110**, 223003 (2013).
17. D. F. Walls, G. J. Milburn, *Quantum Optics* (Springer, 2008).
18. W. Chen *et al.*, *Science* **341**, 768–770 (2013).
19. L. M. K. Vandersypen, I. L. Chuang, *Rev. Mod. Phys.* **76**, 1037–1069 (2005).
20. R. H. Hadfield, *Nat. Photonics* **3**, 696–705 (2009).
21. M. D. Eisaman, J. Fan, A. Migdall, S. V. Polyakov, *Rev. Sci. Instrum.* **82**, 071101 (2011).
22. F. Marsili *et al.*, *Nat. Photonics* **7**, 210–214 (2013).
23. Y. Colombe *et al.*, *Nature* **450**, 272–276 (2007).
24. B. Dayan *et al.*, *Science* **319**, 1062–1065 (2008).
25. C. Junge, D. O'Shea, J. Volz, A. Rauschenbeutel, *Phys. Rev. Lett.* **110**, 213604 (2013).
26. J. D. Thompson *et al.*, *Science* **340**, 1202–1205 (2013).
27. B. Wang, L.-M. Duan, *Phys. Rev. A* **72**, 022320 (2005).
28. A. S. Sørensen, K. Mølmer, *Phys. Rev. Lett.* **91**, 097905 (2003).
29. Y.-F. Xiao *et al.*, *Phys. Rev. A* **70**, 042314 (2004).
30. L.-M. Duan, B. Wang, H. J. Kimble, *Phys. Rev. A* **72**, 032333 (2005).
31. D. L. Moehring *et al.*, *Nature* **449**, 68–71 (2007).
32. C. Nölleke *et al.*, *Phys. Rev. Lett.* **110**, 140403 (2013).

Acknowledgments: We thank N. Kalb for experimental assistance. This work was supported by the European Union (Collaborative Project SIQS) and the Bundesministerium für Bildung und Forschung via IKT 2020 (QK_QuOReP).

Supplementary Materials

www.sciencemag.org/content/342/6164/1349/suppl/DC1
Materials and Methods
Fig. S1

18 September 2013; accepted 5 November 2013
Published online 14 November 2013;
10.1126/science.1246164

Effect of Collective Molecular Reorientations on Brownian Motion of Colloids in Nematic Liquid Crystal

T. Turiv,[1,2] I. Lazo,[2] A. Brodin,[1,3] B. I. Lev,[4] V. Reiffenrath,[5] V. G. Nazarenko,[1] O. D. Lavrentovich[2]*

In the simplest realization of Brownian motion, a colloidal sphere moves randomly in an isotropic fluid; its mean squared displacement (MSD) grows linearly with time τ. Brownian motion in an orientationally ordered fluid—a nematic—is anisotropic, with the MSD being larger along the axis of molecular orientation, called the director. We found that at short time scales, the anisotropic diffusion in a nematic becomes anomalous, with the MSD growing slower or faster than τ; these states are respectively termed subdiffusion and superdiffusion. The anomalous diffusion occurs at time scales that correspond to the relaxation times of director deformations around the sphere. Once the nematic melts, the diffusion becomes normal and isotropic. Our experiment shows that the deformations and fluctuations of long-range orientational order profoundly influence diffusive regimes.

Random displacements of a small particle in a fluid are controlled by kinetic energy dissipation (*1*). The mean displacement is zero but the average mean squared displacement (MSD) is finite, growing linearly with time lag τ (*2*): $\langle \Delta \mathbf{r}^2(\tau) \rangle = 6D\tau$, where D is the translational diffusion coefficient. Brownian particles in complex fluids may exhibit an anomalous behavior, $\langle \Delta \mathbf{r}^2(\tau) \rangle \propto \tau^{\alpha}$, with the exponent α either smaller than 1 (subdiffusion) or larger than 1 (superdiffusion). Subdiffusion is observed in polymer (*3*) and F-actin networks (*4*) and in surfactant dispersions (*5*); superdiffusion occurs in concentrated suspensions of swimming bacteria (*6*) and dispersions of polymer-like micelles (*7*–*10*). The diffusion regimes should reflect the properties of the host medium (*11*), one of which is often a local or long-range orientational order of molecules.

The simplest orientationally ordered fluid is a uniaxial nematic, in which the average orientation of molecules is described by a unit director $\hat{\mathbf{n}}$. Because of different effective viscosities $\eta_{\parallel} \neq \eta_{\perp}$ for motion parallel and perpendicular to $\hat{\mathbf{n}}$, Brownian motion becomes anisotropic, with two coefficients $D_{\parallel}$ and $D_{\perp}$ (*12*–*19*). The anisotropic diffusion characterized experimentally to date for nematics at relatively long time lags τ remains "normal," with $\alpha = 1$ (*14*–*19*). In some cases, anomalous diffusion has also been observed, but it was attributed to features other than the orientational order, such as bacterial activity (*6*), size distribution of building units (*7*), spatial modulation of hydrophobic and hydrophilic regions (*8*), bending rigidity of the molecular aggregates (*8*), fluctuations of concentration (*9*), or director distortions around the dye molecules (*20*). Here, we show that the nematic orientational order and its

[1]Institute of Physics NASU, Prospect Nauky 46, Kyiv 03039, Ukraine. [2]Liquid Crystal Institute, Kent State University, Kent, OH 44242, USA. [3]National Technical University of Ukraine "KPI," Prospect Peremogy 37, Kyiv 03056, Ukraine. [4]Bogolyubov Institute for Theoretical Physics NASU, 14-b Metrolohichna Street, Kyiv 03680, Ukraine. [5]Liquid Crystals Division, Merck KGaA, 64271 Darmstadt, Germany.

*Corresponding author. E-mail: olavrent@kent.edu

fluctuations alone can cause the diffusion to be both anisotropic and anomalous.

We used silica spheres of diameter d = 1.6 to 10 μm with two types of surface alignment (*21*) that set either perpendicular (Fig. 1A) or tangential (Fig. 1B) orientation of $\hat{\mathbf{n}}$. The spheres are placed in a cell with uniform director alignment $\hat{\mathbf{n}}_0$ set by unidirectionally treated bounding plates (*21*). The director distortions around the particle (*22*) cause repulsion from the bounding substrates, so that the colloids levitate in the nematic bulk (fig. S1) (*23*). To minimize experimental errors caused by birefringence, we use the nematic IS-8200 with ultralow birefringence Δn = 0.0015 (fig. S2) (*24*).

The typical measured MSD versus τ dependencies are presented in Fig. 2 for perpendicular anchoring and in fig. S5 for tangential anchoring. In the isotropic phase, at T = 60°C, diffusion is normal with $D = 9.2 \times 10^{-16}$ m^2/s. In the nematic, at T = 50°C, diffusion becomes anisotropic. At relatively long time scales (τ > 20 to 40 s), this anisotropic diffusion is normal because both MSD components, measured for displacements parallel and perpendicular to $\hat{\mathbf{n}}_0$, grow linearly with τ. We find $D_{\parallel} = 1.9 \times 10^{-16}$ m^2/s and $D_{\perp} = 1.4 \times 10^{-16}$ m^2/s for the normally anchored spheres, and $D_{\parallel} = 2.2 \times 10^{-16}$ m^2/s and $D_{\perp} = 1.3 \times 10^{-16}$ m^2/s for tangential anchoring. In all these cases, $\alpha = 1.0 \pm 0.03$. At the times shorter than 20 to 40 s, the MSD versus τ relation becomes nonlinear (Fig. 2A and fig. S5A), signaling anomalous regimes.

To obtain better insight into the different diffusion regimes, we calculated the velocity autocorrelation function (VACF) $C_{v\parallel}(\tau) = \langle v_x(\tau)v_x(0)\rangle$ (*25*, *26*), where v_x is the velocity of the particle along the x axis, and a similar quantity $C_{v\perp}(\tau) = \langle v_y(\tau)v_y(0)\rangle$ for the y direction. For the isotropic melt (Fig. 2D and fig. S5D) and for the long time scales in the nematic, $C_{v\parallel}(\tau)$ and $C_{v\perp}(\tau)$ are close to zero (Fig. 2, B and C, and fig. S5, B and C), as should be the case when $\alpha = 1$. However, when the time steps for the nematic are within a certain interval $\tau_{sup} < \tau < \tau_{sub}$, both $C_{v\parallel}(\tau)$ and $C_{v\perp}(\tau)$ become negative, indicating subdiffusion. At yet shorter times $\tau < \tau_{sub}$, $C_{v\parallel}(\tau)$ and $C_{v\perp}(\tau)$ are positive, reflecting superdiffusion.

Experimentally, one determines τ_{sup} as the time point at which the VACF changes its sign, and τ_{sub}^{min} as the time point at which the function reaches its minimum; τ_{sub} is determined approximately when the deviation from zero exceeds 10^{-17} m^2/s^2 (a typical scatter of VACF data is shown in Fig. 2, B and C). We find that τ_{sup} and τ_{sub}^{min} increase quadratically with the sphere's diameter (Fig. 3).

The dynamic complexity of the director environment around the Brownian particles and finite span (in terms of time lags) make each of the anomalous regimes unlikely to follow a single power law with a fixed value of α. Qualitatively, the existence of slopes in the MSD versus τ dependencies that are smaller than 1 (for $\tau_{sup} < \tau < \tau_{sub}$) and larger than 1 (for $\tau < \tau_{sup}$) is seen in the log-log plot shown in figs. S13D, S14, and S15 (*21*). If we oversimplify the situation and assume a single power law, MSD $\propto \tau^{\alpha}$, for the τ limits identified above, then the best fit for the subdiffusive domain $\tau_{sup} < \tau < \tau_{sub}$ in IS-8200 is achieved for $\alpha_{\parallel} = 0.35 \pm 0.01$ and $\alpha_{\perp} = 0.30 \pm 0.01$; for $\tau < \tau_{sup}$, one obtains $\alpha_{\parallel} = 1.32 \pm 0.01$ and $\alpha_{\perp} = 1.20 \pm 0.01$.

Anomalous diffusion is also featured in the probability distribution of particle displacements. We calculate the probability distribution function $G(\Delta x,\tau)$ for displacements parallel to $\hat{\mathbf{n}}_0$ (Fig. 4) and $G(\Delta y,\tau)$ for the perpendicular component (fig. S16). Both functions show a distinct behavior within different time scales. For the longest time lags, τ = 40 s, $G(\Delta x,\tau)$ coincides with the Gaussian fitting $G_G(\Delta x)$. Such a behavior is characteristic of normal diffusion (*14*, *18*). For the intermediate time lags, τ = 10 s, only the central part of $G(\Delta x,\tau)$ (small displacements) is approximately Gaussian. The probability of finding a large displacement at these time lags is noticeably lower than for the Gaussian distribution. This behavior correlates with the idea of subdiffusion, as the particle remains close to its original position. Finally, for the shortest time lags, τ = 1 s (Fig. 4), large displacements are more probable than with the normal diffusion; this behavior is indicative of superdiffusion.

The nematic IS-8200 is not unique in terms of the observed effects. In an appropriate range of time scales, subdiffusion is also observed in the thermotropic 4′-pentyl-4-cyanobiphenyl (5CB) (figs. S11 and S14) and in the lyotropic chromonic liquid crystal disodium cromoglycate (figs. S12 and S15).

The experiments demonstrate that the effect of orientationally ordered environment on Brownian motion is profound, causing, in addition to anisotropy, anomalous super- and subdiffusion. These two regimes are observed at relatively short time scales that vary with the material, type of anchoring at the particle's surface, size, and displacement direction with respect to $\hat{\mathbf{n}}_0$. Beyond these short time scales, the diffusion becomes normal (but still anisotropic).

The current models of Brownian motion in a nematic (*12*–*14*, *18*) consider the director field around the particle as stationary. The predicted diffusion is normal, albeit anisotropic (*12*–*18*). We attribute the observed anomalous diffusion to the coupling of the sphere's displacements to the director field and its fluctuations—that is, to an intrinsic memory (*27*) of the system associated with the orientational order, as discussed below.

The director field $\hat{\mathbf{n}}(\mathbf{r},t)$ is coupled to the velocity field $\mathbf{v}(\mathbf{r},t)$ of the nematic. Both $\hat{\mathbf{n}}(\mathbf{r},t)$ and $\mathbf{v}(\mathbf{r},t)$ are perturbed by the particle and by the director fluctuations. A perturbation of the director around a colloid of diameter d relaxes within a characteristic time (*28*) $\tau_d \approx \beta^2\eta_{eff}d^2/K$, where β is a numerical coefficient on the order of 1 that describes the length scale ~βd of deformations (*29*), η_{eff} is the effective viscosity, and K is the elastic constant. For IS-8200, $\eta_{eff}/K \approx 10^{11}$ s/m^2 (figs. S7 to S10) (*21*) and thus τ_d is in the range (depending on d) τ_d = 0.1 to 10 s; this is much longer than the time $\rho d^2/\eta \approx 1$ μs needed by the perturbed fluid of density ρ and viscosity $\eta \approx 0.1$ Pa·s to flow over the distance d (*28*). It means that the isotropic hydrodynamic memory is not the reason for anomalous diffusion, consistent with data for the isotropic melt (Fig. 2, A and D, and fig. S5, A and D).

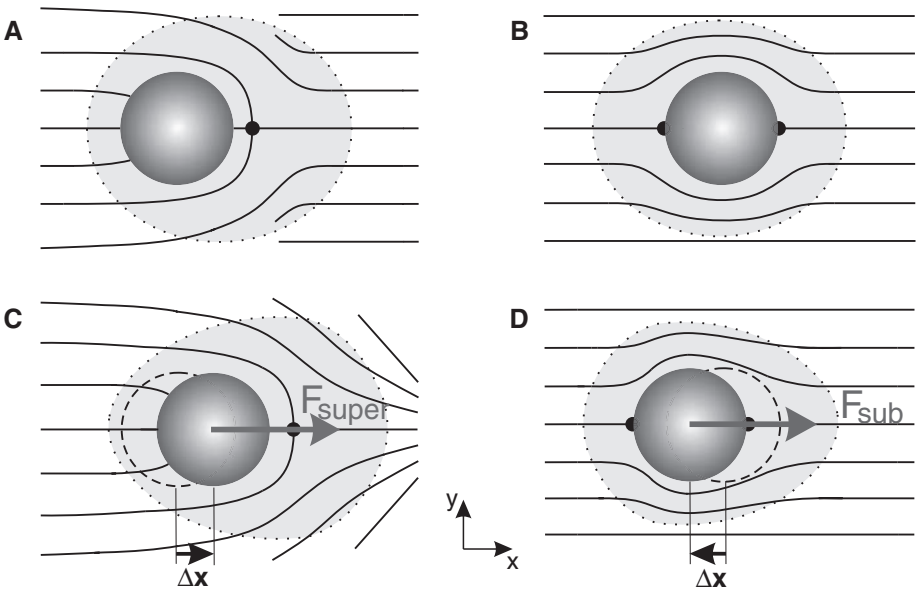

Fig. 1. Director deformations around a sphere and mechanisms of super- and subdiffusion in nematic. (**A** and **B**) Equilibrium director for normal (A) and tangential (B) surface anchoring. (**C**) Elastic force $\mathbf{F}_{super}$ caused by a fluctuative splay on the right side moves the sphere toward the splay. (**D**) Restoring force $\mathbf{F}_{sub}$ responds to displacement $\Delta\mathbf{x}$ that creates stronger director gradients on the left side.

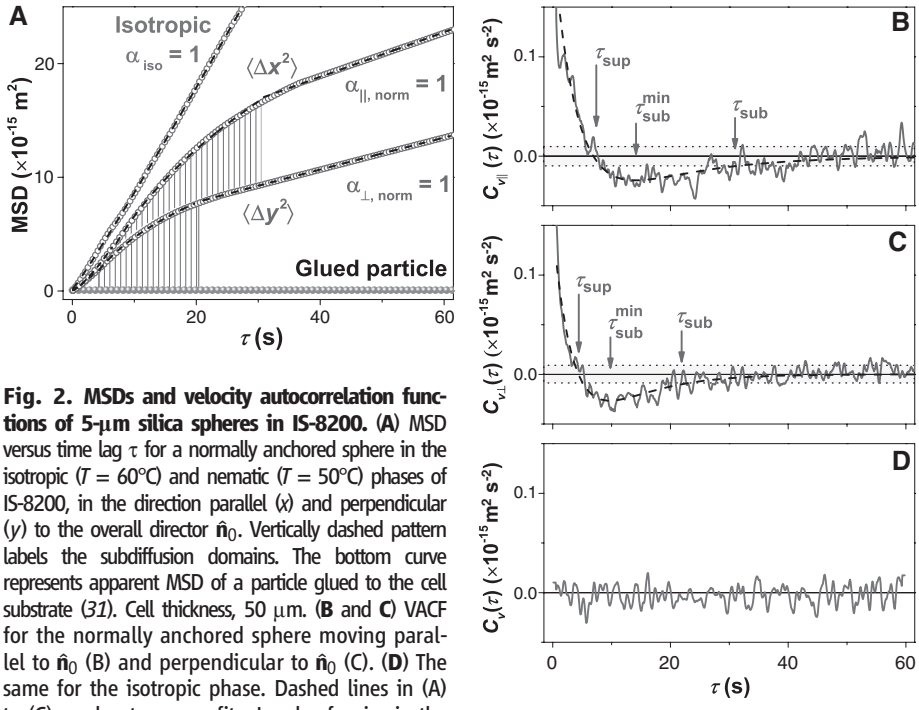

Fig. 2. MSDs and velocity autocorrelation functions of 5-μm silica spheres in IS-8200. (**A**) MSD versus time lag τ for a normally anchored sphere in the isotropic (T = 60°C) and nematic (T = 50°C) phases of IS-8200, in the direction parallel (x) and perpendicular (y) to the overall director $\hat{\mathbf{n}}_0$. Vertically dashed pattern labels the subdiffusion domains. The bottom curve represents apparent MSD of a particle glued to the cell substrate (*31*). Cell thickness, 50 μm. (**B** and **C**) VACF for the normally anchored sphere moving parallel to $\hat{\mathbf{n}}_0$ (B) and perpendicular to $\hat{\mathbf{n}}_0$ (C). (**D**) The same for the isotropic phase. Dashed lines in (A) to (C) are least-squares fits. Levels of noise in the VACF data for the linear domain are shown in (B) and (C) as dotted horizontal lines.

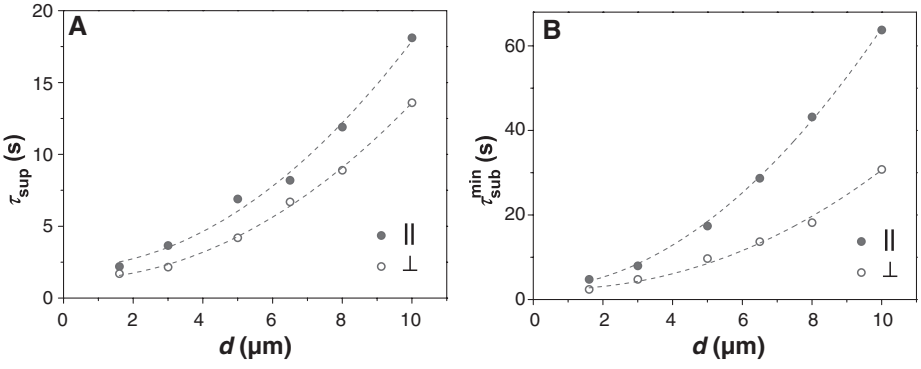

Fig. 3. Characteristic times of anomalous diffusion versus sphere diameter d. (**A** and **B**) Measurements of τ_{sup} (A) and τ_{sub}^{min} (B) for normally anchored spheres in the nematic IS-8200 parallel and perpendicular to $\hat{\mathbf{n}}_0$. Cell thickness, 50 μm; T = 50°C. Dashed lines are quadratic fits.

Fig. 4. Probability distribution of particle displacements parallel to the overall director, for time lags of 1 s, 10 s, and 40 s. Data represent silica spheres (d = 5 μm) with normal anchoring in IS-8200, T = 50°C. The solid lines are Gaussian fits. The data were obtained from a sample of 200,000 single-particle trajectory steps.

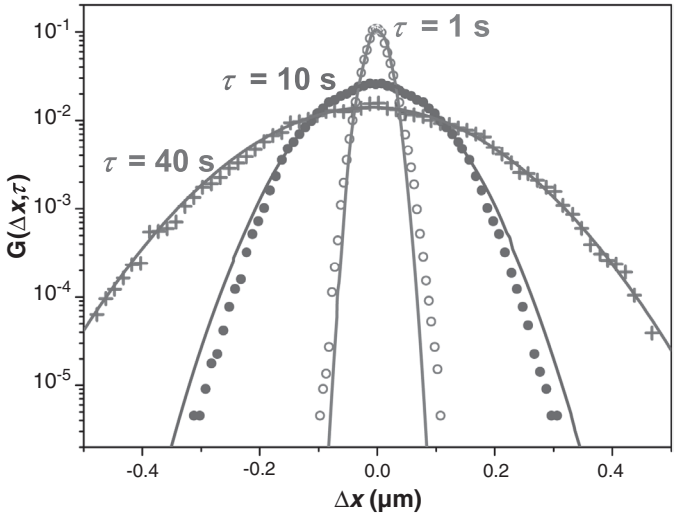

The coupling of director and displacements that leads to subdiffusion at the time scales $\tau_{sub}, \tau_{sub}^{min} \approx \tau_d$ can be illustrated with a tangentially anchored sphere (Fig. 1B). A fluctuative displacement of the sphere, say, to its left by a distance $\Delta\mathbf{x}$ (Fig. 1D) temporarily increases the elastic energy density on the left side and decreases it on the right side. The difference creates a restoring elastic force $\mathbf{F}_{sub} \approx -K\Delta\mathbf{x}/d$ that slows down the diffusive motion.

The case of superdiffusion is sketched in Fig. 1C for a normally anchored sphere that finds itself near a fluctuative splay of the director. The particle experiences an attractive or repulsive force toward the splay, $\mathbf{F}_{super} = -\nabla U$, where $U = -4\pi K \int \mathbf{P}\cdot\mathbf{n}(\nabla\cdot\mathbf{n})dV$ and $\mathbf{P}$ is the elastic dipole of the sphere, $P \propto d^2$ (*29*). This force leads to superdiffusive motion during the lifetime of splay fluctuation.

The memory span in the examples above is determined mostly by τ_d. For $\tau << \tau_d$, the influence of perturbations with wavelength much shorter than d averages to zero. The life span of fluctuations is also limited from above by the cell thickness h, $\tau_h \approx \eta_{eff} h^2/\pi^2 K$. For $h >> d$, the thickness dependence is expected to be weak and dependent on how far from the boundary the sphere levitates (*23*); the latter is determined not only by h but also by densities and by elastic and surface anchoring parameters.

For a sphere with d = 5 μm in an IS-8200 cell of thickness 50 μm, we estimate $\tau_d \approx$ 2.5 s (assuming β = 1 and $\eta_{eff}/K = 10^{11}$ s/m^2) and $\tau_h \approx$ 30 s. These values correlate well with the experimentally found τ_{sup} = 4 to 10 s and τ_{sub} = 20 to 42 s (Fig. 2 and table S2). The quadratic dependence of τ_{sup} and τ_{sub}^{min} on d (Fig. 3) is another strong indication of the director relaxation mechanism.

The considerations above are not restricted to the specific examples in Fig. 1, C and D. For example, a tangentially anchored particle might be attracted by fluctuative deformation in its neighborhood, whereas displacements of a normally anchored sphere would lead to asymmetric director distortions and a subdiffusive slowing. The universality of director distortions (in terms of attraction or repulsion of colloids) is already known for stationary director fields (*30*).

Our work demonstrates that the orientational order in a nematic liquid crystal causes a profound effect on Brownian motion of a small spherical particle and results in anisotropic subdiffusion and superdiffusion. These two phenomena are different from the normal diffusion observed in simple isotropic fluids and from the anisotropic but linear behavior of MSD established for long time scales in liquid crystals. We observe that as the time scale τ decreases, the normal diffusion is replaced by subdiffusion and then by superdiffusion. All three regimes are anisotropic, with different MSDs in the direction parallel to the overall director and perpendicular to it. The characteristic times at which the anomalous regimes are observed are within the range of relaxation times of the director distortions around the particle and director fluctuations.

Although this study dealt with standard liquid crystals, the observed anomalous diffusion is expected to arise in any dispersive environment with orientational order.

References and Notes

1. W. T. Coffey, Y. P. Kalmykov, J. T. Waldron, *The Langevin Equation: With Applications in Physics, Chemistry and Electrical Engineering* (World Scientific, Singapore, 1996).
2. A. Einstein, *Ann. Phys.* **17**, 549 (1905).
3. J. Sprakel, J. van der Gucht, M. A. Cohen Stuart, N. A. M. Besseling, *Phys. Rev. E* **77**, 061502 (2008).
4. I. Y. Wong *et al.*, *Phys. Rev. Lett.* **92**, 178101 (2004).
5. M. M. Alam, R. Mezzenga, *Langmuir* **27**, 6171–6178 (2011).
6. X. L. Wu, A. Libchaber, *Phys. Rev. Lett.* **86**, 557 (2001).
7. A. Ott, J. P. Bouchaud, D. Langevin, W. Urbach, *Phys. Rev. Lett.* **65**, 2201–2204 (1990).
8. Y. Gambin, G. Massiera, L. Ramos, C. Ligoure, W. Urbach, *Phys. Rev. Lett.* **94**, 110602 (2005).
9. R. Ganapathy, A. K. Sood, S. Ramaswamy, *Europhys. Lett.* **77**, 18007 (2007).
10. R. Angelico, A. Ceglie, U. Olsson, G. Palazzo, L. Ambrosone, *Phys. Rev. E* **74**, 031403 (2006).
11. T. G. Mason, D. A. Weitz, *Phys. Rev. Lett.* **74**, 1250–1253 (1995).
12. R. W. Ruhwandl, E. M. Terentjev, *Phys. Rev. E* **54**, 5204–5210 (1996).
13. H. Stark, D. Ventzki, M. Reichert, *J. Phys. Condens. Matter* **15**, S191–S196 (2003).
14. J. C. Loudet, P. Hanusse, P. Poulin, *Science* **306**, 1525 (2004).
15. G. M. Koenig Jr. *et al.*, *Nano Lett.* **9**, 2794–2801 (2009).
16. M. Škarabot, I. Muševič, *Soft Matter* **6**, 5476–5481 (2010).
17. J. A. Moreno-Razo *et al.*, *Soft Matter* **7**, 6828–6835 (2011).
18. F. Mondiot *et al.*, *Phys. Rev. E* **86**, 010401 (2012).
19. D. Abras, G. Pranami, N. L. Abbott, *Soft Matter* **8**, 2026–2035 (2012).
20. M. Pumpa, F. Cichos, *J. Phys. Chem. B* **116**, 14487–14493 (2012).
21. See supplementary materials on *Science* Online.
22. P. Poulin, H. Stark, T. C. Lubensky, D. A. Weitz, *Science* **275**, 1770–1773 (1997).
23. O. P. Pishnyak, S. Tang, J. R. Kelly, S. V. Shiyanovskii, O. D. Lavrentovich, *Phys. Rev. Lett.* **99**, 127802 (2007).
24. V. Reiffenrath, M. Bremer, *Anisotropic Organic Materials* (American Chemical Society, Washington, DC, 2001), pp. 195–205.
25. V. M. Kenkre, R. Kühne, P. Reineker, *Z. Phys. B* **41**, 177–180 (1981).
26. H. Scher, M. Lax, *Phys. Rev. B* **7**, 4491–4502 (1973).
27. N. Kumar, U. Harbola, K. Lindenberg, *Phys. Rev. E* **82**, 021101 (2010).
28. P. G. de Gennes, J. Prost, *The Physics of Liquid Crystals* (Clarendon, Oxford, 1993).
29. T. C. Lubensky, D. Pettey, N. Currier, H. Stark, *Phys. Rev. E* **57**, 610–625 (1998).
30. D. Voloshchenko, O. P. Pishnyak, S. V. Shiyanovskii, O. D. Lavrentovich, *Phys. Rev. E* **65**, 060701 (2002).
31. D. S. Martin, M. B. Forstner, J. A. Käs, *Biophys. J.* **83**, 2109–2117 (2002).

Acknowledgments: We thank R. Kamien, E. I. Kats, T. C. Lubensky, and E. Weeks for fruitful discussions, and O. Boiko, U. Ognysta, and A. Nych for help in the experiments. Supported by NSF grants DMR 1104850 and 1121288, Science & Technology Center in Ukraine project no. 5258, DFFD F35/534-2011, and NASU 1.4.1B/10. See supplementary materials for further details on data.

Supplementary Materials

www.sciencemag.org/content/342/6164/1351/suppl/DC1
Materials and Methods
Supplementary Text
Figs. S1 to S16
Tables S1 and S2
References (*32*–*39*)

16 May 2013; accepted 7 November 2013
10.1126/science.1240591

Detection and Structure of HOON: Microwave Spectroscopy Reveals an O–O Bond Exceeding 1.9 Å

Kyle N. Crabtree,[1] Marat R. Talipov,[2] Oscar Martinez Jr.,[1] Gerard D. O'Connor,[1]* Sergey L. Khursan,[3] Michael C. McCarthy[1]†

Nitric oxide (NO) reacts with hydroxyl radicals (OH) in the gas phase to produce nitrous acid, HONO, but essentially nothing is known about the isomeric nitrosyl-*O*-hydroxide (HOON), owing to its perceived instability. We report the detection of gas-phase HOON in a supersonic molecular beam by Fourier transform microwave spectroscopy and a precise determination of its molecular structure by further spectroscopic analysis of its ^{2}H, ^{15}N, and ^{18}O isotopologs. HOON contains the longest O–O bond in any known molecule (1.9149 ± 0.0005 Å) and appears surprisingly stable, with an abundance roughly 3% that of HONO in our experiments.

Gaseous nitric oxide (NO) is known to undergo association with hydroxyl radicals to generate nitrous acid ($OH^{\bullet} + {}^{\bullet}NO \rightarrow HONO$) (*1*). This elementary step is part of a detailed nitrous acid reaction scheme in the atmosphere, involving soil chemistry, photochemistry, gas-phase reactions, and other heterogenous processes (*2*–*4*); in particular, during the daytime, OH and NO are also regenerated from photolysis of HONO, leading to an association-dissociation cycle. Whereas the aforementioned reaction involves attachment at the nitrogen position of NO, photolysis studies in ice matrices with other radicals have also yielded the isomeric isonitrosyl species: $X^{\bullet} + {}^{\bullet}ON \rightarrow XON$ (X = H, Br, Cl, or CN) (*5*). For the nitrous acid system, such a reaction would generate the isomer nitrosyl-*O*-hydroxide: HOON.

Although this isomer may be formed in the OH + NO reaction, and the higher-energy imine peroxide (HNOO) isomer has been previously observed in ice matrices (*6*, *7*), HOON has never been detected experimentally and has received relatively little attention from theoretical chemists. Perhaps this can be attributed to the results of early calculations, which suggested that HOON is not likely to be stable (*8*), with one study explicitly stating, "[HOON] should be extremely unstable; it is liable to be decomposed to NO + OH with virtually no activation barrier" (*9*). Until very recently, it was only considered as a short-lived, unstable intermediate in the $NH + O_2 \rightarrow OH + NO$ reaction (*9*–*11*) and as a possible dynamical intermediate in highly excited O–H stretching overtones of HONO (*12*). High-level ab initio calculations, however, suggest that the dissociation energy of the O–O bond in HOON is ~8 kcal mol^{-1}, and therefore HOON might be a candidate for matrix isolation studies (*13*).

A striking feature of HOON is its central O–O bond, which calculations have predicted to lie anywhere from 1.5 to 2.0 Å. Uncertainty in both the O–O bond length and stability against dissociation are reminiscent of HO_3, a radical that has received much recent experimental and theoretical attention (*14*–*17*). For HO_3, the central O–O bond length was found to be 1.684 ± 0.003 Å (*15*), considerably longer than a standard O–O single bond—for example, for H_2O_2, r(O–O) = 1.452 Å (*18*)—and its dissociation energy was recently measured to be 2.97 ±0.07 kcal mol^{-1} (*19*). Despite a calculated dissociation energy nearly three times as high as that of HO_3, HOON was most recently predicted to have an O–O bond substantially longer still: 1.89 Å for *trans*-HOON, and 1.91 Å for *cis*-HOON, which lies ~2 kcal mol^{-1} higher in energy (*13*).

Here, we report the detection of the rotational spectrum of *trans*-HOON in the gas phase by means of Fourier-transform microwave (FTM) spectroscopy and double resonance (DR) techniques, as well as a precise determination of its molecular structure by extensive isotopic substitution. The O–O bond length is found to be 1.9149 ± 0.0005 Å, and HOON is formed at roughly 3% of the abundance of HONO under the same conditions, suggesting that this isomer is more stable than previously thought.

HOON was generated in a pulsed supersonic expansion discharge nozzle fed by a gas mixture of NO and water vapor heavily diluted in Ne, a combination known to produce rotationally cold (~2 K) HONO in high abundance (*20*). Both *cis*- and *trans*-HOON are asymmetric rotors close

[1]Harvard-Smithsonian Center for Astrophysics, 60 Garden Street, Cambridge, MA 02138, USA. [2]Department of Chemistry, Marquette University, 535 North 14th Street, Milwaukee, WI 53201, USA. [3]Institute of Organic Chemistry, Ufa Scientific Centre, Russian Academy of Sciences pr. Oktyabra 71, Ufa, 450054 Russian Federation.

*Present address: School of Chemistry, The University of Sydney, New South Wales 2006, Australia.
†Corresponding author. E-mail: mccarthy@cfa.harvard.edu

Effect of Collective Molecular Reorientations on Brownian Motion of Colloids in Nematic Liquid Crystal

T. Turiv, I. Lazo, A. Brodin, B. I. Lev, V. Reiffenrath, V. G. Nazarenko, and O. D. Lavrentovich

Science, **342** (6164), .
DOI: 10.1126/science.1240591

Confusing Colloids in Liquid Crystals

In a simple fluid, particle diffusion such as the motion of colloidal particles shows a change in the mean squared displacement that is proportional with time. Within a nematic liquid crystal, diffusion of the molecules may show anisotropic behavior. Turiv *et al.* (p. 1351; see the Perspective by Abbott) asked what happens to colloidal particles in a nematic liquid crystal. At short times, anomalous diffusion was observed with motion both slower and faster than the long-term behavior, indicative of a complex coupling between the diffusive motion of the colloidal particles and the motion of the liquid crystal molecules.